Eur. Phys. J. C 44, 505–514 (2005)
Digital Object Identifier (DOI) 10.1140/epjc/s2005-02379-5

THE EUROPEAN PHYSICAL JOURNAL C

Production of spin-3 mesons in diffractive DIS

F. Caporale[1], I.P. Ivanov[1,2,a]

[1] INFN, Gruppo Collegato di Cosenza, Università della Calabria, Dipartimento di Fisica, Ponte Bucci, 31C, Arcavacata di Rende (CS), 87036 Italy
[2] Sobolev Institute of Mathematics, Acad. Koptyug avenue, 4, Novosibirsk, 630090, Russia

Received: 1 June 2005 /
Published online: 6 October 2005 –

Abstract. We calculate the amplitudes of $J^{PC} = 3^{--}$ meson production in diffractive DIS within the k_{t}-factorization approach, with particular attention paid to the $\rho_3(1690)$ meson. We find that at all Q^2 the $\rho_3(1690)$ production cross section is 2–5 times smaller than the $\rho(1700)$ production cross section, which is assumed to be a pure D-wave state. Studying σ_{L} and σ_{T} separately, we observe domination of ρ_3 in σ_{L} and domination of $\rho(1700)$ in σ_{T} and offer an explanation of this behavior in simple terms. We also find very strong contributions – sometimes even domination – of the s-channel helicity violating amplitudes. The typical color dipole sizes probed in ρ_3 production are shown to be larger than those in the ground state ρ production, and the energy dependence of ρ_3 cross section turns out to be much flatter than the ρ production cross section. All the conclusions about the relative behavior of the $\rho_3(1690)$ and $\rho(1700)$ mesons are numerically stable against variations of the input parameters.

1 Introduction

Diffractive production of vector mesons (VM) in DIS $\gamma^* p \to Vp$ ($V = \rho, \phi, J/\psi$ etc.) is a very active field of research (see the recent review in [1] and references therein). Studying the Q^2-behavior of the VM production cross sections, one can learn about the transition from soft to hard regimes in the strong interactions, while their energy dependence reveals the Regge properties of the pomeron exchange. The rich set of possible helicity amplitudes $\gamma(\lambda_\gamma) \to V(\lambda_V)$ allows one to study the spin properties of the reaction and to test the s-channel helicity conservation (SCHC).

The main focus of this research has been on the production of the ground state mesons, while diffractive production of excited states did not enjoy much attention. Perhaps, the case studied most so far was the production of radially excited mesons $V(2S)$. The remarkable consequences of the presence of a node in the radial wave function described in [2] were nicely confirmed by H1 measurements of diffractively produced $\psi(2S)$ [3].

Similar experimental studies of excited ρ mesons are expected to be even more rewarding. First, diffractive production of excited ρ mesons probes the dipole cross section at larger dipole sizes than the production of ground states. For example, in the analysis of [4] dipole sizes up to 2 fm were important. Such a unique sensitivity of these reactions to soft diffraction can help to understand the phenomenon of saturation, which is now a hot topic of debates (see [5] and references therein). Another handle offered by diffractive production of ρ' is their possible help in resolving the long standing puzzle of the radial/orbital excitation assignment, as well as a possibility of a hybrid component in the $\rho(1450)$ and $\rho(1700)$ mesons [6].

Diffractive production of excited ρ' mesons has been observed for a long time in a number of fixed target experiments with relatively high energies. Diffractive production of $\rho'(1600)$ was reported in the $\pi^+\pi^-$ [7] and 4π [8] final states (for reanalysis of these data in terms of $\rho(1450)$ and $\rho(1700)$ mesons and for references to earlier experiments at lower energies, see [9]). These states were also studied in the recent Fermilab experiment E687 [10] both in the 2π and 4π channels. Finally, the OMEGA Collaboration has succeeded to measure diffractive photoproduction cross section of the $\rho_3(1690)$ (known then as the $g(1690)$ meson) via the $a_2(1320)\pi \to \eta\pi^+\pi^-$ diffractive final state [11]. However, all these experiments gave only the value of the photoproduction cross section, and no energy dependence, Q^2 dependence, or helicity structure of the reaction was studied. This gap was partially closed by the H1 measurements of the ρ' electroproduction at $4 < Q^2 < 50\,\mathrm{GeV}^2$ [12], but due to low statistics the results presented had large error bars.

Diffractive production of excited states has not received too much attention also from theory. Early theoretical discussions were limited to vector dominance models and its off–forward upgraded versions [9]. The pQCD based calculations of diffractive production of the ground state vector mesons were developed in the mid-90's and were almost immediately extended to the case of radial excitations, since the principal effect there is the presence of the node in the radial wave function [2]. However, for a long time no

[a] e-mail: igivanov@cs.infn.it

microscopic calculation of the orbitally excitated vector mesons was available.

The situation was aggravated by the understanding that production of D-wave vector mesons (as well as $J^{PC} = 3^{--}$ mesons) should be suppressed by Fermi motion, as its radial wave function vanishes at the origin. This suppression was believed to be sufficiently strong and even prompted the authors of [4] to consider diffractive $\rho(1450)$ and $\rho(1700)$ production neglecting in both cases the D-wave contributions altogether. Only in [13] were the S-wave and D-wave vector meson production amplitudes calculated within the $k_{\rm t}$-factorization approach, however at that time the absence of convenient parameterizations of the unintegrated gluon density – the key input quantity – impeded numerical predictions.

During the last years, several fits to the unintegrated gluon density appeared [14, 15]. This allowed for the first estimates [16] of the purely D-wave VM production cross sections, which showed that at small to moderate Q^2 the production rates of the D-wave and $2S$ ρ' states are roughly comparable. This was not surprising, since a similar conclusion was drawn in [9] during the famous splitting of the $\rho'(1600)$ into $\rho(1450)$ and $\rho(1700)$. For a more detailed analysis of the D-wave vector meson production in $k_{\rm t}$-factorization, see [17].

The approach developed in [13] can be applied also to the diffractive production of spin-3 mesons. The D-wave vector meson and the spin-3 meson can be viewed as spin–orbital splitting partners and can be described within the same formalism. The only modification required to proceed from the D-wave VM to the spin-3 meson is that of the $q\bar{q}$ coupling to the final meson:

$$\bar{u}\,\mathcal{D}^{\mu}\,u\cdot V_{\mu}^{*}\to\bar{u}\,\mathcal{C}^{\mu\nu\rho}\,u\cdot T_{\mu\nu\rho}^{*}, \tag{1}$$

where V_μ and $T_{\mu\nu\rho}$ are the polarization vector for the spin-1 and the polarization tensor for the spin-3 mesons, respectively. The spinorial structure $\mathcal{D}^\mu$ determined in [13] corresponds to the pure D-wave vector meson, while the structure $\mathcal{C}^{\mu\nu\rho}$ to be found should correspond to the D-wave spin-3 meson.

In this paper we report the first microscopic derivation of the $J^{PC} = 3^{--}$ production amplitudes within the $k_{\rm t}$-factorization approach. We focus on the $\rho_3(1690)$ production and give predictions on the Q^2 and W dependence of the cross sections, on the $\sigma_{\rm L}/\sigma_{\rm T}$ decomposition, and on the role of s-channel helicity violating amplitudes. We also compare the $\rho_3(1690)$ cross sections with those of $\rho(1700)$, which is assumed to be a purely D-wave vector meson, and observe a number of remarkable distinctions. These should prove useful in disentangling these two mesons in experiment, especially in the case of low statistics.

This paper is organized as follows. In Sect. 2 we show how spin-3 mesons are described and present analytic expressions of the spin-3 meson production amplitudes. In Sect. 3 we perform a twist analysis of the amplitudes in the forward case, compare the results with those of D-wave vector mesons, and discuss the effects of the s-channel helicity violating amplitudes, which will appear in the non-forward scattering. In Sect. 4 we present numerical results for ρ_3 and compare them with the corresponding ground state ρ and $\rho(1700)$ cross sections. In Sect. 5 we discuss the typical color dipole sizes probed in ρ_3 production, compare our results with experimental data available and comment on future possibilities. Finally, in Sect. 6 we draw our conclusions.

2 Amplitudes of spin-3 meson production

2.1 Kinematics and notation

We use the usual notation for the kinematical variables. Q^2 is the photon's virtuality, W is the total center-of-mass energy of the $\gamma^* p$ collision. The momentum transfer from proton to photon is denoted by Δ_μ and at high energies is almost purely transverse: $-\Delta^2 = |t| \approx |t'| = \boldsymbol{\Delta}^2$. The transverse vectors (orthogonal to the $\gamma^* p$ collision axis) will be always labelled by an arrow.

The diffractive production of meson V with mass m_V can be treated in the lowest Fock state approximation as the production of the corresponding $q\bar{q}$ pair of invariant mass $M \neq m_V$, which is then projected, at the amplitude level, onto the final state. Within the leading log $\frac{1}{x}$ accuracy the higher Fock states are reabsorbed into the evolution of the unintegrated gluon density (or color dipole cross section). A typical diagram to be calculated [1] contains the valence quark loop, with integration over the quark transverse momentum $\boldsymbol{k}$ and its fraction of photon's light-cone momentum z, and the uppermost gluon loop, with the integration over transverse momentum $\boldsymbol{\kappa}$. A convenient choice is to assign the momentum $\boldsymbol{k} + z\boldsymbol{\Delta}$ to the quark and $-\boldsymbol{k} + (1-z)\boldsymbol{\Delta}$ to the antiquark, which ensures that even at non-zero $\boldsymbol{\Delta}$ the $q\bar{q}$ invariant mass is $M^2 = \frac{m^2+\boldsymbol{k}^2}{z(1-z)}$. It is also convenient to consider the relative $q\bar{q}$ momentum $p^\mu \equiv (k_q - k_{\bar{q}})^\mu/2$ in the $q\bar{q}$ pair rest frame, where it reduces to the 3-momentum $\mathbf{p} = (\boldsymbol{k}, k_z)$ with $k_z \equiv \frac{2z-1}{2} M$. Such 3-dimensional vectors, which always refer to the $q\bar{q}$ rest frame, will be given in bold.

Finally, throughout the text the ground state vector mesons (which will be always understood as $1S$ states) will be generically labelled by V or V_{1S}; the pure D-wave vector mesons will be labelled by V_D, while the $J^{PC} = 3^{--}$ states of the same quarkonium will be marked as V_3. When we speak of D-wave mesons, we will always assume D-wave *vector mesons*, not spin-3 mesons (although in V_3 the $q\bar{q}$ pair also sits in the D-wave). In order to avoid excessive subscripts, m_V will refer to the mass of the meson being discussed. In particular, for the ρ system we will speak of ρ_3 and ρ_D. The former refers to the physical $\rho_3(1690)$ state, while the identification of the latter with $\rho(1700)$ is clearly model dependent and is done only for purposes of comparison. The effects of S-wave admixture in $\rho(1700)$ are considered in [17].

2.2 Description of a spin-3 meson

A spin-3 particle is described with the rank-3 polarization tensor $T^{\mu\nu\rho}$, which must be symmetric and traceless in

any pair of Lorentz indices. States with any given helicity can be written as simple combinations of the well-known polarization vectors e^μ_λ, $\lambda = +1, 0, -1$ (see below more on e^μ_0):

$$T^{\mu\nu\rho}_{+3} = e^\mu_+ e^\nu_+ e^\rho_+, \qquad T^{\mu\nu\rho}_{+2} = \frac{1}{\sqrt{3}}\{e^\mu_+ e^\nu_+ e^\rho_0\},$$
$$T^{\mu\nu\rho}_{+1} = \frac{1}{\sqrt{15}}\left(2\{e^\mu_+ e^\nu_0 e^\rho_0\} + \{e^\mu_+ e^\nu_+ e^\rho_-\}\right),$$
$$T^{\mu\nu\rho}_{0} = \frac{1}{\sqrt{10}}\left(2e^\mu_0 e^\nu_0 e^\rho_0 + \{e^\mu_+ e^\nu_0 e^\rho_-\}\right), \qquad (2)$$

where curly brackets denote symmetrization.

To construct the spinorial structure $\mathcal{C}^{\mu\nu\rho}$, recall first that both quark and antiquark spinors can be treated on-mass shell (see details in [16]). Therefore, $\mathcal{C}^{\mu\nu\rho}$ can be contructed from two independent structures: $\gamma^\mu p^\nu p^\rho$ and $p^\mu p^\nu p^\rho$ (symmetrization over indices is assumed). When constructing $\mathcal{C}^{\mu\nu\rho}$, we should make sure that it represents a purely $L = 2$ state without admixture of $L = 4$ wave, which is in complete analogy with the construction of S- and D-wave vector mesons performed in [13]. Note that we explicitly rely on the lowest Fock state approximation of the meson; if higher Fock states are taken into account, such a simple picture is lost.

$\mathcal{C}^{\mu\nu\rho}$ in (1) can be constructed in a most transparent way in the non-relativistic case. Instead of the D-wave vector meson structure $\varphi^\dagger D^{ij}\sigma^j\,\varphi$, where $D^{ij} \equiv 3p^i p^j - \delta^{ij}\mathbf{p}^2$, we have now $\varphi^\dagger D^{ij}\sigma^k\,\varphi$. Recall that this structure will be contracted with the polarization tensor T^{ijk} so that one should not worry about symmetrization. Since this polarization tensor is traceless, the coupling simplifies to $\varphi^\dagger\,\sigma^k\,\varphi\,p^i p^j$, which is just a tensor product of the S-wave coupling for vector meson and the $p^i p^j$ term. We do not have to keep track of the overall normalization factors, since they can always be absorbed in the definition of the radial wave function.

Returning to the fully relativistic case, we can now write the spinorial structure for spin-3 meson coupling:

$$\bar u\,\mathcal{C}^{\mu\nu\rho}\,u\cdot T_{\mu\nu\rho} = \bar u\,\mathcal{S}^\mu p^\nu p^\rho\,u\cdot T_{\mu\nu\rho} \equiv \bar u\,\mathcal{S}^\mu\,u\cdot\tau_\mu,$$
$$\tau_\mu \equiv T_{\mu\nu\rho}p^\nu p^\rho. \qquad (3)$$

As the last form of this coupling shows, the spin-3 amplitudes are easy to construct once we know the amplitudes for the S-wave vector meson.

Given the spinorial structure, one can now calculate various amplitudes with the spin-3 meson. In such calculations, the radial wave function $\psi(\mathbf{p}^2)$ will appear, whose normalization is

$$1 = \frac{N_c}{(2\pi)^3}\int \mathrm{d}^3\mathbf{p}\,4M|\psi_3(\mathbf{p}^2)|^2\cdot\left(-\tau^\mu\tau^*_\mu\right)$$
$$= \frac{N_c}{(2\pi)^3}\,\frac{2}{15}\int \mathrm{d}^3\mathbf{p}\,4M\mathbf{p}^4|\psi_3(\mathbf{p}^2)|^2. \qquad (4)$$

Apart from the coefficient 1/15, this normalization condition coincides with the D-wave vector meson normalization condition.

We underline that our approach to describing the polarization states of the final meson is explicitly rotationally invariant. We use *identical* radial wave functions for all the polarization states of the final meson, and in this way the normalization condition (4) holds for an arbitrary polarization state of the spin-3 meson. An important part of the rotation-invariant description is that the transversity condition must be imposed at the level of the $q\bar q$ pair. This leads to the concept of the *running longitudinal* polarization vector $e^\mu_0(M)$, such that it is orthogonal to the 4-momentum of the on-mass shell $q\bar q$ pair with invariant mass M, rather than the momentum of the final meson. The calculations with the fixed longitudinal polarization vector often found in the literature break the rotation invariance. In technical terms, the fixed polarization vector leads to a mixing of the longitudinal spin-1 state and spin-0 states.

Potential models suggest that the radial wave functions of the spin–orbital partners should be very similar. One can assume, as a starting approximation, that their shapes are identical. This assumption leads to

$$\psi_3(\mathbf{p}^2) = \sqrt{15}\,\psi_D(\mathbf{p}^2), \qquad (5)$$

which will be useful for comparison of spin-3 and D-wave vector meson production.

2.3 Generic amplitudes

A generic form of the helicity amplitudes $\gamma^*(\lambda_\gamma)\to V_3(\lambda_3)$ is

$$\mathrm{Im}\,A_{\lambda_3;\lambda_\gamma} = W^2\,\frac{c_V\sqrt{4\pi\alpha_{\mathrm{em}}}}{4\pi^2}\int\frac{\mathrm{d}z\mathrm{d}^2\boldsymbol{k}}{z(1-z)}\int\frac{\mathrm{d}^2\boldsymbol{\kappa}}{\boldsymbol{\kappa}^4} \qquad (6)$$
$$\times\alpha_{\mathrm{s}}\,\mathcal{F}(x_1,x_2,\boldsymbol{\kappa},\boldsymbol{\Delta})\cdot I^{(3)}_{\lambda_3;\lambda_\gamma}\cdot\psi_3(\mathbf{p}^2).$$

Here c_V is the flavor dependent average charge of the quark, the argument of the strong coupling constant α_{s} is $\max[z(1-z)(Q^2+M^2),\boldsymbol{\kappa}^2]$, and $\mathcal{F}(x_1,x_2,\boldsymbol{\kappa},\boldsymbol{\Delta})$ is the skewed unintegrated gluon distribution, with $x_1\neq x_2$ being the fractions of the proton's momentum carried by the uppermost gluons. The appearance of skewed (or generalized) parton distributions is characteristic for scattering processes that change the mass/virtuality of the projectile [18]; see also recent reviews [19]. In the case of meson production, its use is important due to $x_2 \ll x_1$ and has been incorporated in the collinear factorization approach [18,20] as well as in the factorization approach with non-zero transverse momenta of the quarks taken into account [21]. In the k_{t}-factorization approach, the skewness is transferred to the unintegrated distributions.

The integrands for the spin-3 mesons $I^{(3)}_{\lambda_3;\lambda_\gamma}$ can be written in terms of the corresponding integrands for vector mesons:

$$I^{(3)}_{+3;\lambda_\gamma} = I_{+;\lambda_\gamma}(k^*_+)^2, \qquad (7)$$

$$I^{(3)}_{+2;\lambda_\gamma} = \frac{1}{\sqrt{3}}\left(2I_{+;\lambda_\gamma}k_z k^*_+ + I_{0;\lambda_\gamma}(k^*_+)^2\right), \qquad (8)$$

$$I^{(3)}_{+1;\lambda_\gamma} = \frac{1}{\sqrt{15}}\left[(2k_z^2-\boldsymbol{k}^2)I_{+;\lambda_\gamma} + 4k_z k^*_+ I_{0;\lambda_\gamma}\right.$$

$$+(k_+^*)^2 I_{-;\lambda_\gamma}\big]\,, \tag{9}$$

$$I^{(3)}_{0;\lambda_\gamma} = \frac{1}{\sqrt{10}}\left[(2k_z^2-\boldsymbol{k}^2)I_{0;\lambda_\gamma} + 2k_z k_-^* I_{+;\lambda_\gamma} + 2k_z k_+^* I_{-;\lambda_\gamma}\right], \tag{10}$$

where we used shorthand notation

$$k_\pm \equiv -(p_\mu e_\pm^\mu) = \mathbf{p}\cdot\mathbf{e}_\pm = -k_\mp^*,$$
$$k_z \equiv -(p_\mu e_{\rm L}^\mu) = \mathbf{p}\cdot\mathbf{e}_0. \tag{11}$$

Note that both p_μ and e_λ^μ depend on $\boldsymbol{\Delta}$; still this dependence of their scalar product vanishes due to Lorentz invariance. The integrands $I_{\lambda_i;\lambda_\gamma}$ are

$$I_{0;0} = 4QMz^2(1-z)^2\left[1+\frac{(2z-1)^2}{4z(1-z)}\frac{2m}{M+2m}\right]\Phi_2, \tag{12}$$

$$I_{+;+} = m^2\Phi_2 + [z^2+(1-z)^2]\Phi_{1+}k_+^* + \frac{m}{M+2m}\left[\boldsymbol{k}^2\Phi_2 - (2z-1)^2\Phi_{1+}k_+^*\right], \tag{13}$$

$$I_{-;+} = 4z(1-z)\left[1+\frac{(2z-1)^2}{4z(1-z)}\frac{2m}{M+2m}\right]k_+\Phi_{1+} - \frac{2m}{M+2m}k_+^2\Phi_2, \tag{14}$$

$$I_{0;+} = -4z(1-z)\left[1+\frac{(2z-1)^2}{4z(1-z)}\frac{2m}{M+2m}\right]k_z\Phi_{1+} + \frac{2m}{M+2m}k_z k_+\Phi_2, \tag{15}$$

$$I_{+;0} = -4z(1-z)\frac{Q}{M}k_z k_+^*\frac{M}{M+2m}\Phi_2. \tag{16}$$

The integrands for helicity -1 can be obtained from those with $+1$ by replacement of $k_+ \to k_-$ and $\Phi_{1+} \to \Phi_{1-}$ (with no extra minus sign that would appear only at the level of amplitudes!). Here the function Φ_2 describes the transition of a virtual photon into the $q\bar{q}$ states with $\lambda_q + \lambda_{\bar{q}} = \lambda_{\gamma^*}$, whereas $\boldsymbol{\Phi}_1$ describes the transition of transverse photons into the $q\bar{q}$ states with $\lambda_q + \lambda_{\bar{q}} = 0$, in which the helicity of the photon is carried by the orbital angular momentum in the $q\bar{q}$ state:

$$\Phi_2 = -\frac{1}{(\boldsymbol{r}+\boldsymbol{\kappa})^2+\overline{Q}^2} - \frac{1}{(\boldsymbol{r}-\boldsymbol{\kappa})^2+\overline{Q}^2} + \frac{1}{(\boldsymbol{r}+\boldsymbol{\Delta}/2)^2+\overline{Q}^2} + \frac{1}{(\boldsymbol{r}-\boldsymbol{\Delta}/2)^2+\overline{Q}^2}\,,$$
$$\boldsymbol{\Phi}_1 = -\frac{\boldsymbol{r}+\boldsymbol{\kappa}}{(\boldsymbol{r}+\boldsymbol{\kappa})^2+\overline{Q}^2} - \frac{\boldsymbol{r}-\boldsymbol{\kappa}}{(\boldsymbol{r}-\boldsymbol{\kappa})^2+\overline{Q}^2} + \frac{\boldsymbol{r}+\boldsymbol{\Delta}/2}{(\boldsymbol{r}+\boldsymbol{\Delta}/2)^2+\overline{Q}^2} + \frac{\boldsymbol{r}-\boldsymbol{\Delta}/2}{(\boldsymbol{r}-\boldsymbol{\Delta}/2)^2+\overline{Q}^2}\,,$$

where $\boldsymbol{r} \equiv \boldsymbol{k} + (2z-1)\boldsymbol{\Delta}/2$ and $\overline{Q}^2 \equiv z(1-z)Q^2 + m^2$.

3 Large Q^2, m_V^2 analysis

The above expressions can be integrated numerically. However, before describing these results it is useful to study analytically the case where both Q^2 and m_V^2 are much larger than any soft scale, while Q^2/m_V^2 can be arbitrary. In this approximation one expands the hard scale $\overline{Q}^2$ around $\overline{Q}_0^2 \equiv \frac{1}{4}(Q^2+m_V^2)$, and also performs an expansion in powers of a small Fermi motion of the $q\bar{q}$ pair, $k_z^2, \boldsymbol{k}^2 \ll m_V^2$. We will call this approximation the "twist" expansion. We start with the forward case, $\boldsymbol{\Delta}=0$, where only the s-channel helicity conserving amplitudes with $\lambda_3 = \lambda_\gamma$ survive, and find the ratio $\sigma_{\rm L}/\sigma_{\rm T}$ as well as the relation between the V_3 and V_D production cross sections. After this, we discuss the role of the helicity violating amplitudes.

3.1 Twist expansion for the forward case

We consider the two non-zero integrands in this approximation, (9) and (10), and note that after $\mathrm{d}\Omega_{\mathbf{p}}$ angular averaging all terms in each of these expressions give comparable contributions, $\propto \mathbf{p}^4\boldsymbol{\kappa}^2/\overline{Q}_0^4$, differing only by numerical coefficients:

$$I^{(3)}_{+;+} = \frac{\boldsymbol{\kappa}^2}{\overline{Q}_0^4}\mathbf{p}^4\left[\frac{3}{15}\left(1+\frac{8}{3}\frac{M^2}{Q^2+M^2}\right) - \frac{6}{15} + \frac{3}{15}\right] = \frac{\boldsymbol{\kappa}^2}{\overline{Q}_0^4}\cdot\frac{8}{15}\mathbf{p}^4\frac{M^2}{Q^2+M^2},$$

$$I^{(3)}_{0;0} = \frac{Q}{M}\cdot\frac{\boldsymbol{\kappa}^2}{\overline{Q}_0^4}\mathbf{p}^4\left[\frac{2}{15}\left(1+\frac{4M^2}{Q^2+M^2}\right) + \frac{2}{15}\right] = \frac{Q}{M}\cdot\frac{\boldsymbol{\kappa}^2}{\overline{Q}_0^4}\cdot\frac{4}{15}\mathbf{p}^4\left(1+\frac{2M^2}{Q^2+M^2}\right).$$

It is curious to note that the leading-twist contribution in the transverse amplitudes vanishes, and one is left with the subleading term. This cancellation does not occur in the longitudinal amplitude, which leads to an abnormally large value of the ratio $\sigma_{\rm L}/\sigma_{\rm T}$:

$$R_{\rm LT} \equiv \frac{\sigma_{\rm L}}{\sigma_{\rm T}}\cdot\frac{m_V^2}{Q^2} = \frac{27}{8}\left(1+\frac{Q^2}{3m_V^2}\right)^2 \gg 1. \tag{17}$$

This must be confronted with $R_{\rm LT}=1$ for the ground state mesons and, even more remarkably, with $R_{\rm LT} \ll 1$ for D-wave vector mesons, evaluated within the same approximation.

We stress that such a peculiar Q^2 dependence of the ratio $\sigma_{\rm L}/\sigma_{\rm T}$ (17) is entirely due to the heavy-meson approximation we used. Allowing for the longitudinal quark motion will restore the leading-twist contribution to the transverse amplitude. What is expected to remain, however, is the overall smallness of the transverse amplitude and, therefore, a large numerical value of $R_{\rm LT}$.

3.2 Spin-3 versus D-wave vector meson

Within the twist expansion, the V_D and V_3 production amplitudes are proportional to $\int \mathrm{d}^3\mathbf{p}\,\mathbf{p}^4\psi_D(\mathbf{p}^2)$ and $\int \mathrm{d}^3\mathbf{p}\,\mathbf{p}^4\psi_3(\mathbf{p}^2)$, respectively. Assuming (5), one can relate the V_D and V_3 production cross sections. The results for the longitudinal and transverse cross sections, separately, are

$$\frac{\sigma_{\mathrm{L}}^{(3)}}{\sigma_{\mathrm{L}}^{(1)}} = 24\left(\frac{1+\frac{2m_V^2}{Q^2+m_V^2}}{1-\frac{8m_V^2}{Q^2+m_V^2}}\right)^2 \gg 1,$$
$$\frac{\sigma_{\mathrm{T}}^{(3)}}{\sigma_{\mathrm{T}}^{(1)}} = 4\left(\frac{1}{1+\frac{15}{4}\frac{Q^2+m_V^2}{m_V^2}}\right)^2 \ll 1, \qquad (18)$$

where we assumed the masses of the two states to be equal. One sees that the longitudinal cross section is dominated by the V_3 meson, while the transverse one is dominated by V_D. In some sense, these two mesons "mirror" each other: where V_3 is suppressed, V_D dominates and vice versa.

This "mirror" behavior can in fact be understood in simple terms. Consider, for instance, the $T \to T$ transition. Note first that although the integrands for V_D derived in [13] look very differently from those of V_3; they can be written in a form similar to (1): $\bar{u}D^\mu u \cdot V_\mu \equiv \bar{u}S^\mu u \cdot D^{\mu\rho}\cdot V_\rho$, where

$$D^{\mu\rho}\cdot V_+^\rho = -\frac{1}{2}\left[(2k_z^2-\boldsymbol{k}^2)e_+^\mu - 6k_zk_+e_0^\mu + 6(k_+)^2e_-^\mu\right].$$

This should be compared with

$$\tau_{+1}^\mu = \frac{1}{\sqrt{15}}\left[(2k_z^2-\boldsymbol{k}^2)e_+^\mu + 4k_zk_+e_0^\mu + (k_+)^2e_-^\mu\right].$$

The corresponding integrands $I^{(3)}_{+;+}$ and $I^{(1)}_{+;+}$ are

$$I^{(3)}_{+;+} = \frac{1}{\sqrt{15}}\left[(2k_z^2-\boldsymbol{k}^2)I_{+;+} + 4k_zk_+^*I_{0;+} + (k_+^*)^2I_{-;+}\right];$$
$$I^{(1)}_{+;+} = -\frac{1}{2}\left[(2k_z^2-\boldsymbol{k}^2)I_{+;+} - 6k_zk_+^*I_{0;+} + 6(k_+^*)^2I_{-;+}\right]. \qquad (19)$$

The key point is the opposite signs in front of the second term. It turns out that the contributions of all three terms in $I^{(1)}_{+;+}$ are of the same sign and of the same order of magnitude, so that they interfere constructively in V_D production. In the case of V_3, they interfere destructively, which leads to a suppressed $\sigma_{\mathrm{T}}^{(3)}$.

For the longitudinal amplitude, the similar change of signs strongly suppresses the result for D-wave mesons, enhancing it in the spin-3 case. We see that there are good reasons to expect such a "mirror" behavior of V_3 and V_D just on the basis of their spin–angular composition.

3.3 The role of s-channel helicity violation

The approximate conservation of the s-channel helicity in diffractive reactions is due to two reasons. First, in diffraction the helicity properties of the target and projectile are uncorrelated, and in the forward case strict SCHC holds separately for the projectile and the target. At $\boldsymbol{\Delta} \neq 0$ the s-channel helicity non-conserving (SCHNC) amplitudes depend on the momentum transfer as $|\boldsymbol{\Delta}|^{|\lambda_\gamma-\lambda_V|}$, which makes them small within diffractive cone. Second, at high energy the helicity is conserved at the parton level, so in order to produce helicity flip the transverse motion of constituent must come into play. This produces extra factors like $\boldsymbol{k}^2/M^2$, further suppressing helicity violation, especially for heavy quarks. Nevertheless, a small violation of SCHC has been observed at HERA in the case of light vector mesons; at the amplitude level, its relative magnitude was estimated to be ∼10% [22].

In the case of V_3 production, the effect of SCHNC must be more important, just as it was for D-wave vector meson production [17]. The integration of the quadrupole term kills the leading contribution to the SCHC amplitudes (12) and (13), and the SCHC amplitudes get the same suppression due to Fermi motion as SCHNC ones. Moreover, partial cancellation among several terms discussed above suppresses the $T \to T$ amplitude, while the helicity violating amplitudes do not suffer such cancellation. Finally, one may pay attention to numerical factors like $1/\sqrt{15}$ in the amplitude $A_{+1;+1}$, which are absent, for example, in the $A_{+3;+1}$ amplitude and take into account the large number of various helicity violating amplitudes for spin-3 meson production.

Thus, one can anticipate that the helicity violating amplitudes can generate a significant portion of the overall cross section. One should not even be surprised to see them dominate in the transverse cross section, especially at small Q^2. Therefore, the above twist analysis is meant only to guide the eye and should not be used for a quantitative discussion.

4 Numerical study

In this section we present numerical results for the particular case of ρ_3 production.

4.1 Input

In order to integrate (6) numerically, one needs to specify models for the unintegrated gluon density and the meson wave function. We related the skewed unintegrated gluon density with non-zero momentum transfer to the forward unintegrated gluon density by

$$\mathcal{F}\left(x_1, x_2, \boldsymbol{\kappa}+\frac{1}{2}\boldsymbol{\Delta}, -\boldsymbol{\kappa}+\frac{1}{2}\boldsymbol{\Delta}\right)$$
$$= \mathcal{F}\left(0.41\frac{Q^2+m_V^2}{W^2}, \boldsymbol{\kappa}\right)\exp\left(-\frac{b_{3\mathbb{P}}\boldsymbol{\Delta}^2}{2}\right), \qquad (20)$$

where $b_{3\mathbb{P}}$ includes contributions from the two-gluon form-factor of the proton and from the effective pomeron trajectory, as described in detail in [1]. Although fixing the exact numerical value of the shift coefficient (0.41) is beyond

the $\log \frac{1}{x}$ accuracy, its introduction is phenomenologically motivated and, after all, it can be viewed as yet another parameter in our parametrization. We did not try varying this parameter to obtain a better fit. The parametrizations for the forward unintegrated gluon density were borrowed from [15]. Note that the k_t-factorization approach itself does not require Q^2 to be large, and in the soft region, $Q^2 \lesssim 1\,\mathrm{GeV}^2$, the words "unintegrated gluon density" should be understood simply as an appropriately normalized Fourier transform of the dipole cross section.

As for the radial wave function, we choose the simple Gaussian Ansatz WF normalized according to (4), with the only free parameter, the "size" a of the wave function. In contrast to the vector meson case, dileptonic decay $\rho_3 \to e^+e^-$ cannot proceed via one-photon annihilation and does not help us fix a. However, appealing to the argument that the radial wave functions of spin–orbital partners should be similar, we can take $a_3 = a_D$, the latter being extracted from $\Gamma(\rho(1700) \to e^+e^-)$.

4.2 Level of accuracy anticipated

Our experience with diffractive production of ground state vector mesons within the same approach tells us that variation of the input parameters changes the absolute values of the cross sections by a factor of $\lesssim 1.5$, while the accuracy for the observables that depend on the *ratios* of the amplitudes is even better [1, 16]. The principal source of uncertainty was found to be the final meson wave function, especially its density near the origin. The sensitivity of the results to the particular parametrizations of the unintegrated gluon density presented in [16] (from both DGD2000 and DGD2002 sets of parametrizations) was found to be weak.

In the present case, the results are expected to be less stable with variation of input due to the presence of various cancellations. The main source of instability is the poorly known value of the ρ_D dileptonic decay width. The data available give $\Gamma(\rho_D \to e^+e^-) \sim 0.1$–$0.6\,\mathrm{keV}$ (assuming that $\rho(1700)$ is indeed the D-wave $q\bar{q}$ state). The possibility that $\rho(1700)$ has significant contributions from radially excited $q\bar{q}$ and from a possible hydrid state, as well as taking into account extremely large NLO corrections [23] for this decay, makes the situation even less definite.

All the curves to be presented below were calculated for $\Gamma(\rho_D \to e^+e^-) = 0.14\,\mathrm{keV}$. This value corresponds to the value of $\Gamma(e^+e^-)\cdot\mathrm{Br}(\pi^+\pi^-) = 29^{+16}_{-12}\,\mathrm{eV}$ obtained in [24]. In order to see the effect of this input parameter, we calculated cross sections both for ρ_3 and ρ_D for the dileptonic decay width in the interval 0.14–0.7 keV. Increasing $\Gamma(\rho_D \to e^+e^-)$, we observed some suppression of the cross sections at small Q^2 and their significant growth at $Q^2 \gtrsim 1\,\mathrm{GeV}^2$, especially in the case of σ_T. The effect is strong, and we conclude that the numerical results for the *absolute values* of the cross sections are reliable only within factors of ∼2–3.

We stress, however, that variation of the input parameters produced absolutely the same shifts in the ρ_D production cross sections. This should be expected, because the relation between the two mesons is dictated primarily by the similarity of their radial distributions and by spin–angular relations of type of (19). These relations are essentially insensitive to details of the model, as long as we treat $\rho(1700)$ as a predominantly $q\bar{q}$ pair in the D-wave state. We conclude therefore that the numerical values of our predictions for ratios between ρ_3 and ρ_D are more stable, approximately within a factor of 1.5–2.

4.3 Q^2 and t dependence

We calculated all the helicity amplitudes (7)–(10) for the spin-3 meson and compared its production rate with that of ρ_D and ρ_{1S}. All the cross sections are calculated at $W = 75\,\mathrm{GeV}$ and are obtained from numerical integration of the differential cross sections within the region $0 < |t| < 1.05\,\mathrm{GeV}^2$.

Figure 1 shows the ratios of the excited to ground state meson cross sections $\sigma(\rho_3)/\sigma(\rho_{1S})$ and $\sigma(\rho_D)/\sigma(\rho_{1S})$. Both ratios are an order of magnitude smaller than unity, and the ρ_D cross section is noticeably larger than that of ρ_3, especially at $Q^2 \sim 1\,\mathrm{GeV}^2$. At larger Q^2, the ratio $\sigma(\rho_D)/\sigma(\rho_3) \sim 2$. Thus, if one intends to extract the $\rho(1700)$ properties from diffractively produced multipion states around an invariant mass of ∼1700 MeV, one cannot neglect contamination by the ρ_3 state.

The difference between ρ_D and ρ_3 is better seen if one studies separately the longitudinal and transverse cross sections, shown in Fig. 2. Here, the solid and dash-dotted lines represent the ρ_3 and ρ_D cross sections, respectively. In the case of ρ_3 we showed also with the dashed lines the contributions of the SCHC amplitudes only. One clearly sees the

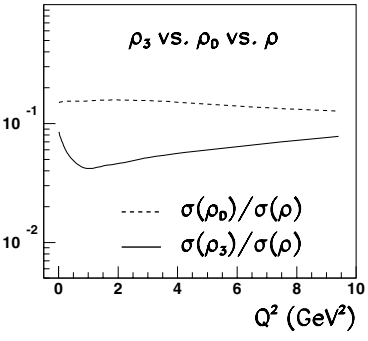

Fig. 1. Predictions for the ratios of ρ_3 (solid line) and ρ_D (dashed line) to the ρ production cross sections as a function of Q^2

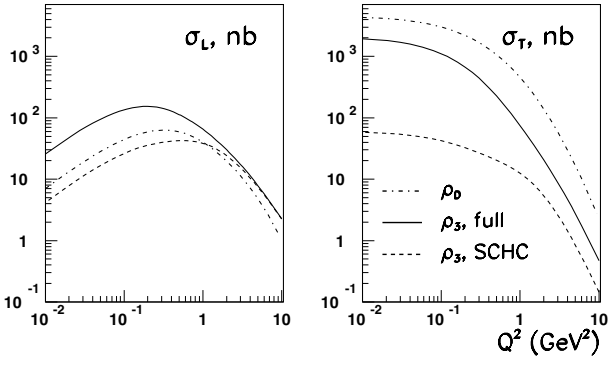

Fig. 2. Predictions for the longitudinal (left plot) and transverse (right plot) cross sections of ρ_3 (solid lines) and ρ_D (dash-dotted lines) production. The contribution to ρ_3 from the SCHC amplitudes only is shown with dashed lines

domination of helicity violating amplitudes at small Q^2 in ρ_3 production. One can even state, on the basis of our calculations, that ρ_3 production at small Q^2 *probes diffraction in the regime of strong s-channel helicity violation*. In the case of the longitudinal cross section, the contribution of SCHNC transitions becomes small at $Q^2 > 1\,\mathrm{GeV}^2$, since all such amplitudes are of higher twist. Helicity violation remains strong for transverse photons even at large Q^2.

As mentioned above, in the case of D-wave vector mesons one expects suppression of σ_L but not of σ_T. Indeed, our calculations show the domination of the ρ_3 over ρ_D in σ_L at small $Q^2 \lesssim 1\,\mathrm{GeV}^2$, while in σ_T the ρ_D cross section is noticeably larger than ρ_3 everywhere. This is in qualitative agreement with the twist analysis result (18).

Such a different behavior of ρ_D and ρ_3 can be seen also in the plots of the ratio $\sigma_\mathrm{L}/\sigma_\mathrm{T}$ as a function of Q^2, shown in Fig. 3. Here, on the left plot, we showed this ratio for ρ_3 and ρ_D, while on the right plot, we showed reduced ratios $R_\mathrm{LT} = \frac{\sigma_\mathrm{L}}{\sigma_\mathrm{T}} \cdot \frac{m_i^2}{Q^2}$, where m_i is the mass of the corresponding meson. R_LT is small for ρ_D and relatively large for ρ_3, as was expected from the twist analysis (17). We note that the region $Q^2 \sim 1\,\mathrm{GeV}^2$ is particularly suitable for distinguishing among various ρ states.

The role of helicity violating amplitudes can be seen also in the $|t|$-distributions shown in Fig. 4 for $Q^2 = 1\,\mathrm{GeV}^2$ separately for longitudinal and transverse cross sections. The dashed and dotted lines show the SCHC contributions only, while the solid lines show their sums. As can be expected, the large contributions of SCHNC amplitudes come from the entire t-interval shown, while the SCHC amplitudes are strong only within a narrow forward cone.

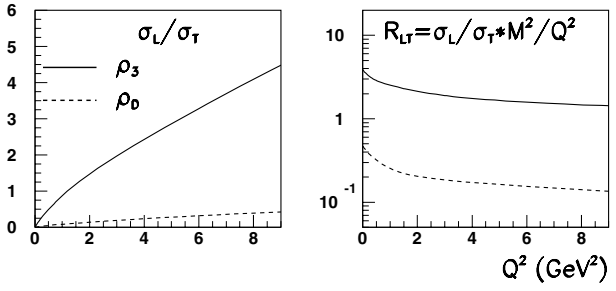

Fig. 3. Predictions for the ratios of the longitudinal to transverse cross sections of ρ_3 (solid line) and ρ_D (dashed line) production. The left plot shows $R = \sigma_\mathrm{L}/\sigma_\mathrm{T}$, while the right plot shows the reduced ratio $R_\mathrm{LT} = \sigma_\mathrm{L}/\sigma_\mathrm{T} \cdot m_V^2/Q^2$

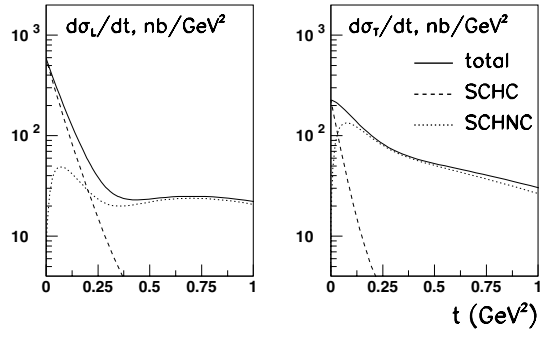

Fig. 4. Differential cross sections $\mathrm{d}\sigma_\mathrm{L}/\mathrm{d}|t|$ (left plot) and $\mathrm{d}\sigma_\mathrm{T}/\mathrm{d}|t|$ (right plot) for ρ_3 at $Q^2 = 1\,\mathrm{GeV}^2$ as functions of $|t|$. The dashed and dotted lines show contributions from helicity conserving and helicity violating amplitudes, respectively; the solid lines show their sum

4.4 Energy dependence

We checked also the energy dependence of the ρ_3 production cross section, which we parametrized with a simple power law $\sigma(\rho_3) \propto W^\delta$. General expectations, driven by the ground state production experience [1], are that at small Q^2 this exponent should be a small number, and one speaks usually of a "soft pomeron", while in the presence of a hard scale it should grow up to $\delta \sim 1$, corresponding to the "hard pomeron".

For a particular example, we used HERA kinematics and studied the energy behavior of the cross section within the range $W = 50$–$200\,\mathrm{GeV}$. We found that at small to moderate Q^2, the ρ_3 production cross section (both longitudinal and transverse) slightly *decreases* with energy increase, with typically $\delta \sim -0.1$ to -0.2. It is only at $Q^2 \gtrsim 5\,\mathrm{GeV}^2$ that δ becomes positive, and it is always smaller than the value of δ for the corresponding ground state vector meson.

This decrease is naturally understood in the Regge picture of the pomeron exchange. The differential cross section at non-zero t behaves roughly as

$$\frac{\mathrm{d}\sigma}{\mathrm{d}t} \propto W^{\delta(t)};$$
$$\delta(t) = 4[\alpha_\mathbb{P}(t) - 1] \approx 4[\alpha_\mathbb{P}(0) - 1 - \alpha'_\mathrm{eff} \cdot |t|].$$

The value of the effective pomeron intercept $\alpha_\mathbb{P}(0)$ depends on Q^2 and comes directly from the parametrizations of the forward unintegrated gluon density [15]. At small Q^2 it is about $\alpha_\mathbb{P}(0) - 1 \sim 0.08$, and starts noticeably growing only at $Q^2 \gtrsim 2$–$3\,\mathrm{GeV}^2$. The effective slope of the pomeron trajectory is $\alpha'_\mathrm{eff} \approx 0.12\,\mathrm{GeV}^{-2}$ with a very marginal Q^2 dependence. (Note that it differs from the fixed input parameter $\alpha'_\mathrm{eff} \approx 0.25\,\mathrm{GeV}^{-2}$ used in our calculations due to anti-shrinkage effects discussed in detail in [25].) Thus, the effective exponent of the energy dependence of the integrated cross section

$$\delta \approx 4[\alpha_\mathbb{P}(0) - 1 - \alpha'_\mathrm{eff} \cdot \langle|t|\rangle]$$

is governed not only by $\alpha_\mathbb{P}(0)$, but also by the typical momentum transfers $\langle|t|\rangle$ involved.

In the production of ground state vector mesons the dominant contribution comes from SCHC helicity amplitudes, which are concentrated within the forward cone $|t| \lesssim 0.1\,\mathrm{GeV}^2$. In the present case, as Fig. 4 shows vividly, the range of important values of $|t|$ spans up to 0.5–1 GeV^2. One sees that due to such high values of $|t|$ involved the energy increase exponent δ at small Q^2 can easily become negative.

5 Discussion

5.1 What dipole sizes are probed in ρ_3 photoproduction?

The S-wave $q\bar{q}$ state is naturally orthogonal to the D-wave $q\bar{q}$ state. For example, if one attempts to calculate the inelastic $\rho_S \to \rho_D$ formfactor at zero momentum transfer, one finds

$$\mathcal{M} \propto \int \frac{\mathrm{d}z}{z(1-z)} \mathrm{d}^2\boldsymbol{k}\, \psi_D^*(\mathbf{p}^2)\psi_S(\mathbf{p}^2)(2k_z^2 - \boldsymbol{k}^2)$$
$$= \int \frac{4}{M} \mathrm{d}^3\mathbf{p}\, \psi_D^*(\mathbf{p}^2)\psi_S(\mathbf{p}^2)(2k_z^2 - \boldsymbol{k}^2) = 0.$$

The presence of the quadrupole combination $2k_z^2 - \boldsymbol{k}^2$ makes the amplitude zero, as long as all other factors under the integral are spherically symmetric.

In the photoproduction, the wave function of the initial photon is not spherically symmetric, but one can still appeal to the vector dominance model arguments and rewrite the ρ_3 photoproduction amplitude as

$$\langle\gamma|\sigma(r)|\rho_3\rangle \propto g_{\gamma\rho} \cdot \langle\rho|\sigma(r)|\rho_3\rangle. \qquad (21)$$

One can suspect that a similar orthogonality should be at work here, when one considers a forward SCHC amplitude at large $q\bar{q}$ dipole sizes, where the dipole cross section $\sigma(r) \to$ const so that all other factors seemingly become spherically symmetric. If this were the case, it would mean that the ρ_3 photoproduction receives little contribution from large dipoles and is a "harder" process than the ρ photoproduction. However, this is not the case. The most essential difference between the $\rho p \to \rho_3 p$ amplitude and (6) is the replacement of the photon wave function:

$$\Phi_2 \to \Psi_2$$
$$= \frac{1}{z(1-z)} \left[2\psi_S(k_z^2 + \boldsymbol{k}^2) - \psi_S(k_z^2 + (\boldsymbol{k}+\boldsymbol{\kappa})^2)\right.$$
$$\left. - \psi_S(k_z^2 + (\boldsymbol{k}-\boldsymbol{\kappa})^2)\right], \qquad (22)$$

together with a similar replacement of $\boldsymbol{\Phi}_1$. For clarity, we explicitly presented the spherically symmetric quantity $\mathbf{p}^2$ as $k_z^2 + \boldsymbol{k}^2$. At small values of $\boldsymbol{\kappa}^2$, which correspond to large dipole sizes, one obtains

$$\Psi_2 \approx -2\boldsymbol{\kappa}^2 \left[\psi_S'(\mathbf{p}^2) + \boldsymbol{k}^2\psi_S''(\mathbf{p}^2)\right], \qquad (23)$$

where derivatives of the radial wave function are taken with respect to $\mathbf{p}^2$.

The result (23) explicitly lacks spherical symmetry. Thus, even if one uses the leading-twist contributions, pretending that the $\rho \to \rho_3$ transition is well approximated by non-relativistic expressions, one still gets

$$\int \mathrm{d}^3\mathbf{p} \left[\psi_S'(\mathbf{p}^2) + \boldsymbol{k}^2\psi_S''(\mathbf{p}^2)\right] \psi_3 \cdot (2k_z^2 - \boldsymbol{k}^2) \neq 0. \qquad (24)$$

This result is rather natural. The characteristic feature of the high-energy collision is the presence of a preferred direction: that of the proton's momentum in the vector meson rest frame. The transverse and longitudinal dynamics of the quark loop now differ, and this leads, in particular, to circulation of purely transverse momentum $\boldsymbol{\kappa}$ in the loop, see (23), which breaks the spherical symmetry. Taking into account the Fermi motion makes the expression to be integrated even less symmetric.

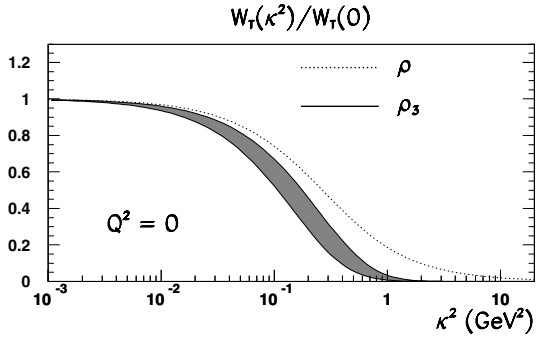

Fig. 5. The mapping functions $W_\mathrm{T}(\boldsymbol{\kappa}^2)$ normalized to the $\boldsymbol{\kappa}^2 = 0$ point for the ρ_3 (solid lines) and ρ_{1S} (dotted line) photoproduction. The shaded area shows the distribution of the results due to the decay width variation $\Gamma(\rho_D \to e^+e^-) = 0.14$–$0.7\,\mathrm{keV}$

It is useful to check explicitly that large dipoles indeed contribute substantially to the ρ_3 production amplitude. In order to test this numerically, we change the order of integration in (6) and represent the forward $T \to T$ amplitude as

$$\frac{1}{W^2}\,\mathrm{Im}\,A_{+1;+1} = \int \frac{\mathrm{d}\boldsymbol{\kappa}^2}{\boldsymbol{\kappa}^2} \mathcal{F}(x_1, x_2, \boldsymbol{\kappa}, 0) \cdot W_\mathrm{T}(\boldsymbol{\kappa}^2). \qquad (25)$$

One expects $W_\mathrm{T}(\boldsymbol{\kappa}^2)$ to have the "smoothed step function" shape: it should be approximately constant at small $\boldsymbol{\kappa}^2$ up to some value $\overline{Q_\mathrm{T}}^2$, and should decrease quickly as $\boldsymbol{\kappa}^2$ passes this value, see [26] for details of this analysis for the ground state ρ production. This function "cuts out" the important range of gluon momenta, and determines thus the important range of the color dipole sizes. The effect of orthogonality – if it were present – would appear in $W_\mathrm{T}(\boldsymbol{\kappa}^2)$ as a small-$\boldsymbol{\kappa}^2$ suppression.

In Fig. 5 we show $W_\mathrm{T}(\boldsymbol{\kappa}^2)$ normalized to the $\boldsymbol{\kappa}^2 = 0$ point for the ρ_3 and ρ_{1S} photoproduction with solid and dotted lines, respectively. The shaded area corresponds to scattering of the results due to variation of the decay width $\Gamma(\rho_D \to e^+e^-) = 0.14$–$0.7\,\mathrm{keV}$. We observe no small-$\boldsymbol{\kappa}^2$ suppression for ρ_3. The $\boldsymbol{\kappa}^2$ value where $W(\boldsymbol{\kappa}^2)/W(0)$ hits $1/2$ is $\boldsymbol{\kappa}^2 \approx 0.1$–$0.2\,\mathrm{GeV}^2$ for the ρ_3, and is noticeably smaller than the corresponding value of $0.27\,\mathrm{GeV}^2$ in the ρ_{1S} production. One sees that the ρ_3 production is indeed a softer process, and the typical dipole sizes probed are $\sim 1.2 \div 1.5$ times larger than in the ground state VM production.

5.2 Comparison with experimental data available

The OMEGA Collaboration at CERN measured the cross section of diffractive photoproduction of $\rho_3(1690)$ (known

then as the $g(1690)$ meson) via the $a_2(1320)\pi$ subsample of the $\eta\pi^+\pi^-$ diffractive final state events [11]. The cross section of $\gamma p \to \rho_3(1690)p \to a_2(1230)\pi p$ was found to be $97 \pm 28 \pm 21$ nb, which allows one to roughly estimate the ρ_3 production cross section as $\sigma(\gamma p \to \rho_3(1690)p) \sim 200$–$300$ nb. This result is about 5–10 times below our photoproduction predictions, which we think is not a very bad discrepancy, taking into account the expected level of accuracy in the soft region. Indeed, most of this cross section we predict to be due to SCHNC, especially the double-flip, transitions. Its magnitude in the soft region was predicted by our calculation to be rather large even for ground state vector mesons, but so far has been poorly known from experiment. We think that upon understanding better the role of SCHNC at small Q^2 with the aid of modern experiments, we can improved the accuracy of our predictions. We expect, however, that our conclusion of the strong violation of s-channel helicity violation probed in ρ_3 will survive such an upgrade. In addition, our cross sections correspond to integration within $0 < |t| < 1.05\,\mathrm{GeV}^2$; the results will change noticeably if one selects another t-interval.

The OMEGA Collaboration also measured the photoproduction cross section of ρ'. The original data were reanalyzed in terms of $\rho(1450)$ and $\rho(1700)$ separately in [9] yielding $\sigma(\rho(1700)) \sim 500$ nb. Thus, our result $\sigma(\rho(1700))/\sigma(\rho_3) \sim 3$ at the photoproduction limit is roughly consistent with experiment. Finally, comparing the ρ_3 and the ground state ρ photoproduction cross sections, we note that our result $\sigma_3/\sigma_{1S} \sim 0.1$ is again not very far from the experimental value of 0.02–0.03.

5.3 Comments on experimental possibilities

The experimental analysis of diffractive production of spin-3 resonances, and in particular, the strategy of $\rho_3(1690)/\rho(1700)$ separation, will depend on the statistics available and the final state chosen.

Should one have the luxury of high statistics, one can do the partial wave analysis or select some particular final states, in which one of the two states would dominate. An example of this approach is just the OMEGA Collaboration observation of the ρ_3 in the $a_2(1320)\pi \to \eta\pi^+\pi^-$ final state. If the statistics does not allow for such an angular dependence or final state analysis, one then should look for distinctions in the production of these mesons. In the view of our results, it is tempting to make use of ratios $\sigma_\mathrm{L}/\sigma_\mathrm{T}$, which are dramatically different for ρ_3 and ρ_D, especially in the small to moderate Q^2 region.

One possibility to separate σ_L and σ_T is given by the Rosenbluth method. It will require several runs at different lepton beam energies and might seem impractical at high energies. The second possibility could be to do a baby-version of PWA and to study angular correlations in final state hadrons. For example, if both mesons discussed are observed in $\pi^+\pi^-$ (the corresponding branching ratios are not dominant, but still sizable), one could study the single-differential angular distribution $W(\cos\theta)$. This measurement will give spin density matrix element r^{04}_{00}, from which one recovers $\sigma_\mathrm{L}/\sigma_\mathrm{T}$. Alternatively, one can search for a similarly revealing angular dependence in 4π final states, the dominant decay channel of both mesons.

Another issue, which requires taking into account the ρ_3 meson, is the recent observation of a narrow dip structure in diffractively photoproduced $3\pi^+3\pi^-$ states at $M_{6\pi} \approx 1.9$ GeV in the Fermilab E687 experiment [27]. Although the detailed mechanism of its appearance remains unsettled, the very recent analysis [28] sees it as a result of the interplay of several resonances with $J^{PC} = 1^{--}$ (including $\rho(1700)$) and a background. This analysis was explicitly based on the vector dominance idea and explicitly uses the assumption that the 6π spectra in e^+e^- annihilation and in diffractive photoproduction are essentially the same (apart from kinematical factors). The results presented here clearly show that this is a risky assumption. The ρ_3 meson does not couple to the single virtual photon, yet it should be produced diffractively at a rate comparable to that of $\rho(1700)$. Although it cannot produce any interference pattern with $J = 1$ states, its own contribution can affect the results of the very delicate analysis of [28].

6 Conclusions

We calculated the cross section of the exclusive production of $J^{PC} = 3^{--}$ mesons in diffractive DIS within the k_t-factorization approach. The results were compared with the cross section of the D-wave state vector meson of the same quarkonium. We exemplified the general expressions with a detailed numerical study of the ρ system, where the $\rho_3(1690)$ state is almost degenerate with the $\rho(1700)$ meson, whose structure is arguably dominated by the $q\bar{q}$ pair in the D-wave.

The absolute values of the cross sections suffer from uncertainties of the input parameters, in particular, of the $\rho_D \to e^+e^-$ decay width, and we can be sure only of the order of magnitude of these results. However, in what concerns the relative production rates of ρ_3 and ρ_D, our conclusions are much more certain. Our results allow us to formulate the following predictions, which are stable against variations of the model parameters.

(1) In typical HERA kinematics, the ratio of production cross sections taken at equal Q^2 is $\sigma(\rho_D)/\sigma(\rho_3) \approx 3$–$5$ at small Q^2, decreasing to ≈ 2 at larger Q^2. Thus, when extracting the properties of $\rho(1700)$ from multipion final states, one cannot simply neglect the ρ_3 contribution.

(2) ρ_3 and ρ_D show completely different patterns in σ_L–σ_T decomposition: ρ_3 dominates in the longitudinal cross section, while ρ_D dominates in the transverse cross section. The ratios $R = \sigma_\mathrm{L}/\sigma_\mathrm{T}$ for ρ_3 and ρ_D differ by more than one order of magnitude. This dramatic difference can be traced back to the spin–angular properties of these two mesons, see (19).

(3) The role of the s-channel helicity violating amplitudes is extremely important, especially in the transverse cross section. At small to moderate Q^2 the helicity violating amplitudes even dominate over the SCHC ones. Thus, production of ρ_3 offers an interesting possibility to study diffraction in the regime of strong s-channel helicity violation.

(4) Due to the large color dipole sizes probed in the ρ_3

production and the large region of relevant momentum transfers, $|t| \lesssim 1\,\mathrm{GeV}^2$, the energy dependence of the ρ_3 production cross section is less steep than in the case of ρ. At small Q^2, one might even observe a decrease of the ρ_3 cross section with energy increase.

We find no surprise in the numerical stability of the first two conclusions, since they are essentially driven by very basic relations: similarity of the radial wave functions for ρ_3 and ρ_D, the spin–angular composition of these mesons, see (19), and the quadrupole suppression of the leading contributions in the SCHC amplitudes (12) and (13).

In addition, confronting our predictions for photoproduction with the fixed target data available and observing them to agree within the anticipated accuracy inspires hope that we grasp the essential physics of this reaction in our approach. We are looking forward to seeing experimental checks of our predictions.

Acknowledgements. It is our pleasure to acknowledge fruitful discussions with Etienne Burtin, Roberto Fiore, Nicole d'Hose, Dima Ivanov, Kolya Nikolaev, Alessandro Papa, Andrzej Sandacz. The work of I.P.I. is supported by the INFN Fellowship, and partly by INTAS and grants RFBR 05-02-16211 and NSh-2339.2003.2.

References

1. I.P. Ivanov, N.N. Nikolaev, A.A. Savin, hep-ph/0501034; submitted to Phys. Elem. Part. Atom. Nucl.
2. J. Nemchik et al., J. Exp. Theor. Phys. **86**, 1054 (1998) [Zh. Eksp. Teor. Fiz. **113**, 1930 (1998)]; J. Nemchik et al., Z. Phys. C **75**, 71 (1997); J. Nemchik, N.N. Nikolaev, B.G. Zakharov, Phys. Lett. B **339**, 194 (1994)
3. C. Adloff et al. [H1 Collaboration], Phys. Lett. B **541**, 251 (2002); C. Adloff et al. [H1 Collaboration], Phys. Lett. B **421**, 385 (1998)
4. G. Kulzinger, H.G. Dosch, H.J. Pirner, Eur. Phys. J. C **7**, 73 (1999)
5. K. Golec-Biernat, Acta Phys. Polon. B **35**, 3103 (2004)
6. D.V. Bugg, Phys. Rept. **397**, 257 (2004)
7. D. Aston et al., Phys. Lett. B **92**, 215 (1980)
8. D. Aston et al., Nucl. Phys. B **189**, 15 (1981); M. Atkinson et al. [Omega Photon Collaboration], Phys. Lett. B **108**, 55 (1982); M. Atkinson et al. [Omega Photon Collaboration], Z. Phys. C **26**, 499 (1985)
9. A. Donnachie, H. Mirzaie, Z. Phys. C **33**, 407 (1987)
10. P. Lebrun [E687 Collaboration], FERMILAB-CONF-97-387-E, talk given at the 7th International Conference on Hadron Spectroscopy (Hadron 97), Upton, NY, 25–30 August 1997
11. M. Atkinson et al. [Omega Photon Collaboration], Z. Phys. C **30**, 531 (1986)
12. H1 Collaboration, paper pa01-088, submitted to ICHEP 96, Warsaw 1996 (Poland)
13. I.P. Ivanov, N.N. Nikolaev, JETP Lett. **69**, 294 (1999)
14. A.I. Shoshi, F.D. Steffen, H.G. Dosch, H.J. Pirner, Phys. Rev. D **66**, 094019 (2002)
15. I.P. Ivanov, N.N. Nikolaev, Phys. Rev. D **65**, 054004 (2002)
16. I.P. Ivanov, PhD thesis, hep-ph/0303053
17. F. Caporale, I.P. Ivanov, Phys. Lett. B **622**, 55 (2005)
18. A.V. Radyushkin, Phys. Lett. B **385**, 333 (1996); Phys. Rev. D **56**, 5524 (1997); X.D. Ji, Phys. Rev. D **55**, 7114 (1997)
19. A.V. Belitsky, A.V. Radyushkin, hep-ph/0504030; M. Diehl, Phys. Rept. **388**, 41 (2003)
20. J.C. Collins, L. Frankfurt, M. Strikman, Phys. Rev. D **56**, 2982 (1997)
21. S.V. Goloskokov, P. Kroll, hep-ph/0501242
22. C. Adloff et al. [H1 Collaboration], Eur. Phys. J. C **13**, 371 (2000); J. Breitweg et al. [ZEUS Collaborations], Eur. Phys. J. C **12**, 393 (2000); B. Clerbaux, talk given at the Workshop of Low x physics, June 1999, Tel-Aviv, Israel, hep-ph/9908519
23. W. Celmaster, Phys. Rev. D **19**, 1517 (1979); R. Barbieri, R. Kogerler, Z. Kunszt, R. Gatto, Nucl. Phys. B **105**, 125 (1976)
24. L.M. Kurdadze et al., JETP Lett. **37**, 733 (1983) [Pisma Zh. Eksp. Teor. Fiz. **37**, 613 (1983)]
25. I.P. Ivanov, hep-ph/0304089
26. I.P. Ivanov, Phys. Rev. D **68**, 032001 (2003)
27. P.L. Frabetti et al. [E687 Collaboration], Phys. Lett. B **514**, 240 (2001)
28. P.L. Frabetti et al., Phys. Lett. B **578**, 290 (2004)